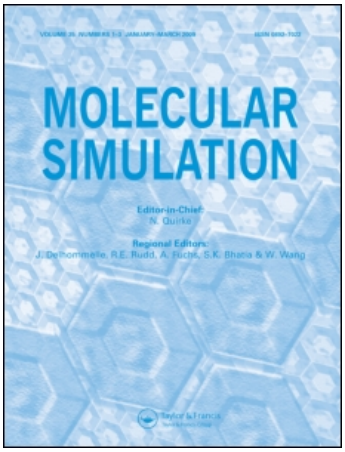

Molecular Simulation
Publication details, including instructions for authors and subscription information:
http://www.informaworld.com/smpp/title~content=t713644482

The Structural and Electronic Properties of Liquid aluminium-Transition Metal Alloys

L. Do Phuong[ab]; D. Nguyen Manh[ab]; A. Pasturel[a]
[a] Laboratoire de Physique Numérique, Maison des Magistères, Grenoble, France [b] Department of Physics, Polytechnic University of Hanoi, Vietnam

To cite this Article Phuong, L. Do , Manh, D. Nguyen and Pasturel, A.(1997) 'The Structural and Electronic Properties of Liquid aluminium-Transition Metal Alloys', Molecular Simulation, 20: 1, 79 — 94
To link to this Article: DOI: 10.1080/08927029708024169
URL: http://dx.doi.org/10.1080/08927029708024169

Molecular Simulation, 1997, Vol. 20, pp. 79–94
Reprints available directly from the publisher
Photocopying permitted by license only

THE STRUCTURAL AND ELECTRONIC PROPERTIES OF LIQUID ALUMINIUM-TRANSITION METAL ALLOYS

L. DO PHUONG*, D. NGUYEN MANH* and A. PASTUREL

Laboratoire de Physique Numérique, Maison des Magistères, CNRS BP 166, 38042 Grenoble, France

(Received November 1996; Accepted December 1996)

The structural and electronic properties of liquid Aluminium-Transition metal alloys are studied within the framework of the Tight-Binding (TB) approximation. The atomic structure is calculated using molecular dynamics simulations based on effective interatomic forces derived from a tight-binding-bond (TBB) approach built on a Bethe lattice. The electronic structure is calculated self-consistently using the same tight-binding Hamiltonian but coupled with the recursion method. It is shown that the bond-order depends strongly on the strength of the pd hybridization in the AB alloy, leading to non-additive potentials with a strong preference for the formation of pair of unlike atoms and short bond-distances in the A-B pairs. This is illustrated by studying the electronic and structural properties of liquid $Al_{80}Ni_{20}$ and $Al_{80}Mn_{20}$ alloys and by comparing our results with the available experimental ones.

Keywords: Alloys; tight-binding approximation

I. INTRODUCTION

With the development of simulation techniques in the past two decades, there have been many studies of the properties of various liquid systems. However, an accurate simulation of the properties of transition metals and of their alloys is still a challenging problem since bonding is not well described by currently available pair and embedded-atom potentials [1]. The aim of the embedded-atom approach [2] is to absorb the complex many-atom interactions in the embedding potentials, their form being

*Permanent address: Department of Physics, Polytechnic University of Hanoi, Vietnam.

justified within effective-medium theory [3] or within the second-moment approach [4]. Embedded-atom potentials encounter serious difficulties when applied to the transition metals with a half-filled d band. These difficulties can be overcome in an alternative approach developed by Pettifor [5] in the tight-binding-bond (TBB) model derived from first principles within density-functional theory. In this model, an angular-dependent many-body potential expression for the bond order, which gives the direct dependence of the bond strength on the local atomic environment, can be obtained. The explicit analytic form of these many-body potentials has the necessary ingredients for an adequate description, but there are difficulties in practice when it comes to incorporating the charge transfer contribution between different orbitals in a self-consistent manner. Whereas there is strong evidence that the contributions of multi-ion terms are necessary in the study of solid transition metals, it is believed that progress in the understanding of their liquid state properties may only come about by using effective pair potentials that take accurate account of the important of sp-d hybridization and self-consistent charge transfer contributions.

The last remark has encouraged us to develop a new simple effective pair interaction for liquid transition metals [6]. The bond order is calculated from the tight-binding scalar cluster Bethe lattice method (SCBLM) which is expected to be valid in disordered systems. Indeed, for a disordered system, the detailed structure in the electronic density of states which is the origin of the characteristic variations in the higher moments and hence in the many-body interactions is smeared out. Therefore, it is possible to use approximation such as the cluster Bethe lattice method which gives the correct fourth moment of the local density of states (DOS) and then reproduces the band-mixing effect correctly. In this way, we hope that the TB bond contribution derived from this model will be improved in comparison with the embedding potential through the second moment approximation.

In this paper, our approach is generalized to liquid Aluminium-transition metal (Al-M) alloys. It turns out that the bond orders depend very sensitively on the partial densities of states (DOS) in the alloy. As the electronic density of states Al-M alloys is characterized by a strong hybridization between the sp orbitals of Aluminium and the d-orbitals of transition metal, the pair forces in the alloy are essentially non-additive potentials with a strong preference for the formation of pairs of unlike atoms and short bond distances in the Al-M pairs. In the liquid structure this is reflected in a strong chemical and topological short-range order. We note that our approach is the first to reproduce a quantum-mechanical force field for liquid Al-M alloys which can be used in atomistic simulations.

II. TIGHT-BINDING-BOND APPROACH TO INTERATOMIC FORCES

II.1. Total Energy

The total energy derived from first principles within the density functional theory can be written in the form [7].

$$U_{\text{Tot}} = U_{NN} + U_{DC} + U_{\text{band}} \tag{1}$$

where the first two terms are the contribution from the nuclear-nuclear interactions and the double-counting correction for the electron-electron interaction. U_{band} is the covalent band energy which results from computing the local density of states (LDOS) $n_{i\alpha}(E)$ associated with orbital α on site i.

$$U_{\text{band}} = \sum_{i\alpha} \int^{EF} n_{i\alpha}(E)\, E dE \tag{2}$$

Using the stationary property of the total energy with respect to variations of the true ground-state charge density, Harris [8] and Foulkes [9] showed that $(U_{NN} + U_{DC})$ is describable, to first order in the charge density, as a pair-potential term. Transforming the one-electron Hamiltonian to a two-center orthogonal form shows that the band energy may be measured relative to a reference energy $E_{i\alpha}$, equal to the free-atom energy level $\varepsilon_{i\alpha}$ shifted by a crystal field and a nonorthogonality term. Grouping the crystal-field contribution with the nuclear-nuclear and double-counting terms allows the total energy to be decomposed explicitly in terms of physically intuitive contributions as:

$$U_{\text{Tot}} = U_{\text{atom}} + U_{es} + U_{xc} + U_{no} + U_{\text{bond}} \tag{3}$$

where U_{es} is an electrostatic energy arising from the interaction of the overlapping atomic charge densities, U_{xc} and U_{no} are the exchange-correlation and non-orthogonality contributions, respectively. U_{es}, U_{xc}, and U_{no} may be cast into the form of a repulsive pair-potential term leading to an expression for the binding energy of the form [7]:

$$U_{\text{bind}} = U_{\text{Tot}} - U_{\text{atom}} = U_{\text{rep}} + U_{\text{bond}} \tag{4}$$

U_{bond} is the covalent bond energy:

$$U_{\text{bond}} = \sum_{i\alpha} \int^{EF} (E - E_{i\alpha}) ni\alpha(E) dE \tag{5}$$

$$= U_{\text{band}} - \sum_{i\alpha} N_{i\alpha} E_{i\alpha}$$

which differs from the band energy by the on-site terms which have been grouped with the ionic and double-counting terms.

Equation (4) is derived with the assumption that each atom is assumed to remain charge neutral by varying the on-site Hamiltonian matrix elements in such a way that the energy splittings between different orbitals on the same atom are preserved. This approximation ensures that the TBB model is consistent with the force theorem. It can be shown [10] that with this constraint, the change in the bond energy is to first order equal to the change in the band energy with fixed $E_{i\alpha}$:

$$\Delta U_{\text{bondl}/\Delta Ni\alpha = 0} = \Delta U_{\text{bandl}/\Delta Ei\alpha = 0} \tag{6}$$

II.2. Bethe-lattice Approach to the Bond-order

The bond energy may be broken down in term of contributions from individual pairs of bonds [7] by writing Equation (5) as:

$$U_{\text{bond}} = \frac{1}{2} \sum_{i,j,i \neq j} U^{i,j}_{\text{bond}} \tag{7}$$

where

$$U^{i,j}_{\text{bond}} = 2 \sum_{\alpha,\beta} H_{i\alpha, j\beta} \Theta_{i\alpha, j\beta} \tag{8}$$

where the prefactor 2 accounts for spin degeneracy, H is the tight-binding matrix linking the orbitals on sites i and j together and Θ is the corresponding bond order matrix whose elements are defined at energy E as:

$$\Theta_{j\beta, i\alpha}(E) = -\frac{2}{\pi} \text{Im} \langle j\beta | (E + i0 - H)^{-1} | i\alpha \rangle \tag{9}$$

We note here that, for a self-adjoint representation of H(that is the tight-binding Hamiltonian), we can obtain:

$$\mathrm{Im}\langle j\beta|(E+i0-H)^{-1}|i\alpha\rangle = \frac{1}{2}\mathrm{Im}[\langle\varphi_+|(E+i0-H)^{-1}|\varphi_+\rangle - \langle\varphi_-|(E+i0-H)^{-1}|\varphi_-\rangle] \tag{10}$$

where

$$\varphi_\pm = \frac{1}{\sqrt{2}}(\varphi_{j\beta} \pm \varphi_{i\alpha})$$

Equation (10) allows us to find again the definition of bond order given by Pettifor, by using the bonding G_+ and antibonding G_- Green's functions [5]. Here, we write the bond order in terms of the imaginary part of the off-diagonal Green functions.

$$\Theta_{j\beta,i\alpha} = \int^{EF} \Theta_{j\beta,i\alpha}(E)\,dE = -\frac{2}{\pi}\int^{EF} \mathrm{Im}\,G_{ij}^{\alpha\beta}(E)\,dE \tag{11}$$

In disordered systems such as liquids, instead of the LDOS $n_{i\alpha}(E)$ or of the Green function $G_{ij}^{\alpha\beta}(E)$, we are interested only in configuration-averaged values. In order to calculate these quantities, we have used the SCBLM. One assumes that the mean local environment is isotropic and then there is a spherical point symmetry for the CBLM mean field model [11]. This method is efficient to study s-d hybridization effects in disordered systems; in particular, one can use it to explain the positive Hall coefficient in some transition metal disordered systems [12]. In order to obtain the bond order in the SCBLM formalism we first recall the matrix expression of the Green function of an atom in CBLM [11]:

$$G_I^{CBLM}(z) = \left[z_1 - E_I - Z\sum_J p_{IJ}t_{IJ}S_{IJ}(z)\right]^{-1} \tag{12}$$

where I (i) denotes the species (A or B) at site i, p_{IJ} are the pair probabilities and t_{IJ} and S_{IJ} are the matrix of hopping energies and the so-called transfer matrix respectively. In the spherical approximation made by SCBLM, we obtain simple scalar equations for the Green function in the subspaces $\alpha(i)$

of atom i as [6]:

$$G_{\alpha(i)}(z) = \left[z - E_{\alpha(i)} - Z \sum_{\beta(j)} \sigma^2_{\alpha(i),\beta(j)} G'_{\beta(j)}(z) \right]^{-1} \tag{13}$$

where one defines:

$$\sigma^2_{\alpha(i),\beta(j)} = Z p_{IJ} n_\beta T^2_{\alpha(i),\beta(j)} \tag{14}$$

with n_β is the degeneracy of subspace β and $T^2_{\alpha(i),\beta(j)}$ is the mean square of the matrix element between a state of subspace α of atom i and a state of subspace β of atom j (See Eq. (10) in [11]). Finally $G'_{\beta(j)}(z)$ can be defined by:

$$G'_{\beta(j)} = \left[z - E_{\beta(j)} - \sum_{\gamma(k)} \sigma'^2_{\beta(j),\gamma(k)} G_{\gamma(k)}(z) \right]^{-1} \tag{15}$$

with

$$\sigma'^2_{\beta(j),\gamma(k)} = \frac{Z-1}{Z} \sigma^2_{\beta(j),\gamma(k)}$$

By comparing (12) with (13) and (14) it follows that:

$$t_{\alpha(i)\beta(j)} S_{\beta(j)\alpha(i)}(z) = n_\beta T^2_{\alpha(i)\beta(j)} G'_{\beta(j)}(z) \tag{16}$$

On the other hand, the transfer matrix S is related to the off-diagonal Green function by:

$$\begin{aligned} G_{\beta(j)\alpha(i)}(z) &= \sum_\alpha S_{\beta(j)\alpha(i)} G_{\alpha(i)\alpha(i)}(z) \\ &= n_\alpha S_{\beta(j)\alpha(i)} G_{\alpha(i)}(z) \end{aligned} \tag{17}$$

Then, the bond potential can be written as:

$$U^{ij}_{\text{bond}} = -\frac{2}{\pi} \sum_{\alpha\beta} t_{\alpha(i)\beta(j)} \operatorname{Im} \int^{EF} n_\alpha S_{\beta(j)\alpha(i)}(E) G_{\alpha(i)}(E) dE$$

$$= -\frac{2}{\pi}\sum_{\alpha\beta}\mathrm{Im}\int^{EF} n_\alpha n_\beta T^2_{\alpha(i)\beta(j)} G_{\alpha(i)}(E) G'_{\beta(j)}(E) dE$$

$$= \sum_{\alpha\beta}\Phi^{\mathrm{bond}}_{\alpha(i)\beta(j)} \tag{18}$$

From Eq. (18) it is clear that, in our formalism, the bond potential interaction can be expressed directly from the local Green function treated in the mean isotropic environment. The advantage of Eq. (18) is that it allows us to estimate the different orbital contributions in the bond energy and, in particular, to treat the effect of hybridization explicitly.

Assuming that the bond order $\Phi_{j\beta,i\alpha}$ in Eq. (11) is a slowly varying function of the bond length, we obtain:

$$\Phi^{\mathrm{bond}}_{\alpha(i)\beta(j)} = t_{\alpha(i)\beta(j)}\Theta_{j\beta,i\alpha} \tag{19}$$

with the distance dependence of the hopping integral $t_{\alpha(i)\beta(j)}$. Here the average hopping integrals are evaluated according to Harrison's power law dependence [12]:

$$(ll'm) = \eta_{ll'm}\frac{h^2}{mr^2} \tag{20}$$

for s, p electrons and

$$(ll'm) = \eta_{ll'm}\frac{h^2}{mr^{l+l'+1}}$$

for other electrons.

II. 3. Tight-Binding-Bond (TBB) Potentials

To determine the repulsive part of the total energy, we assume repulsive pairwise interactions $\Phi^{\mathrm{rep}}_{IJ}(r_{ij})$ given by:

$$\Phi^{\mathrm{rep}}_{IJ}(r_{ij}) = \sum_{\alpha,\beta}\Phi^{\mathrm{rep}}_{\alpha(I)\beta(J)}(r_{ij}) = \frac{1}{2}\sum_{\alpha,\beta}\left(\frac{C_{\alpha(I)}C_{\beta(J)}}{r_{ij}^{m_\alpha+m_\beta}}\right)^{1/2} \tag{21}$$

For s-s and p-p interactions, the repulsive pair interaction is modeled as $\Phi^{\mathrm{rep}}_{\alpha\alpha}(r_{ij}) = C_{\alpha\alpha}/r^4_{ij}$ while for d-d interactions, a stronger power-law dependence

C_{dd}/r_{ij}^{10} is chosen. $C_{\alpha\alpha}(\alpha = \text{s, p or d orbitals})$ are the only parameters of the model; they are determined from the knowledge of the experimental atomic volume and bulk modulus of the pure metals. To treat the alloying effect, i.e. the Al-M interactions, we have to determine the attractive and the repulsive parts of the heteroatomic bond potential. The parametrization of the repulsive pair interaction is still achieved using equation (21) with the same $C_{\alpha(A)}$ and $C_{\beta(B)}$ values. To obtain the $h_{A\alpha,B\beta}$ hopping integrals (i.e. $(ss\sigma)_{AB}$, $(sp\sigma)_{AB}$, $(sd\sigma)_{AB}$, $(pd\sigma)_{AB}$ and $(pd\pi)_{AB}$), we use the geometrical average of hopping integrals given in Table I, which is reasonable in the case of the alloys studied. Consequently, no parameters are introduced to describe the alloy properties. At the end, the dependence for both hopping integral and repulsive terms has been modified using the rescaling method proposed by Goodwin *et al.* [14]. This method is known for generating improved TB parameters which are both transferable and suitable for extensive molecular dynamics simulations. The two scaling parameters of the scaling smoothed step-function, i.e. r_c and n_c, have been chosen in such a way that the step is positioned between the first and the second nearest neighbors in the fcc lattice and that the interactions become zero at $L/2$, where L is the linear dimension of the molecular dynamic cell. Table I shows all the parameters entering the interatomic interactions.

III. STRUCTURE OF LIQUID $Al_{80}Ni_{20}$ AND $Al_{80}Mn_{20}$ ALLOYS

III. 1. Structure of Pure Metals

In order to test the validity of our interatomic interactions, we have chosen to study structural and electronic properties of the pure Al, Mn and Ni liquid metals. We have used our interatomic interactions in a standard microcanonical NVE molecular dynamics (MD) investigation of liquid structure of the pure metals. Our molecular dynamics routines are based on integrating the equations of motion in a velocity form of the Verlet algorithms [15]. A 1332-particle cluster with periodic boundary

TABLE I Tight-binding and repulsive parameters for Al, Mn, and Ni (in eV)

	sss	*dds*	*ddp*	*ddd*	*sds*	*pps*	*ppp*	*sps*	*Css*	*Cdd*	*Cpp*
Al	−0.52					1.20	−0.31	0.71	0.30		0.30
Mn	−1.33	−0.65	0.32	0.00	−1.15				1.22	0.07	
Ni	−1.42	−0.56	0.28	0.00	−1.11				0.31	0.07	

conditions is used and the lattice parameter of the molecular dynamics cell is expanded to give the required liquid density. The time increment h in our simulations is chosen to be approximately 10^{-15} s. The liquid is then "heated" by raising initial temperature and subsequently scaling it down to the required value. Typical simulations run up to 3–4. 10^4 steps.

The pair correlation functions $g(r)$ are calculated after averaging over about 250–300 independent configurations taken at intervals at 100 time steps. In Figure 1, as an example, we present the comparison of the pair correlation function with the experimental data for molten aluminium. Note that our molecular dynamics simulations achieve a good fit to the diffraction data for the transition metals (see Ref. [6] for more details) as well as for Aluminium. We have also calculated the electronic density of states of these molten metals, from the atomic coordinates obtained by molecular dynamics simulations. Using the same tight-binding Hamiltonian, the recursion method has been used and we have stopped the recursion after about 12 levels of the continued fraction for s, p and d orbitals. For transition metals, the global behaviour of the total DOS is dominated by the d-band contribution, the s-d hybridization leading to a decrease in the s-DOS inside the d-band as has been shown by Mayou *et al.* [11]. The total DOS of liquid Aluminium (see Fig. 2) is very similar to the ones of the sp-bonded

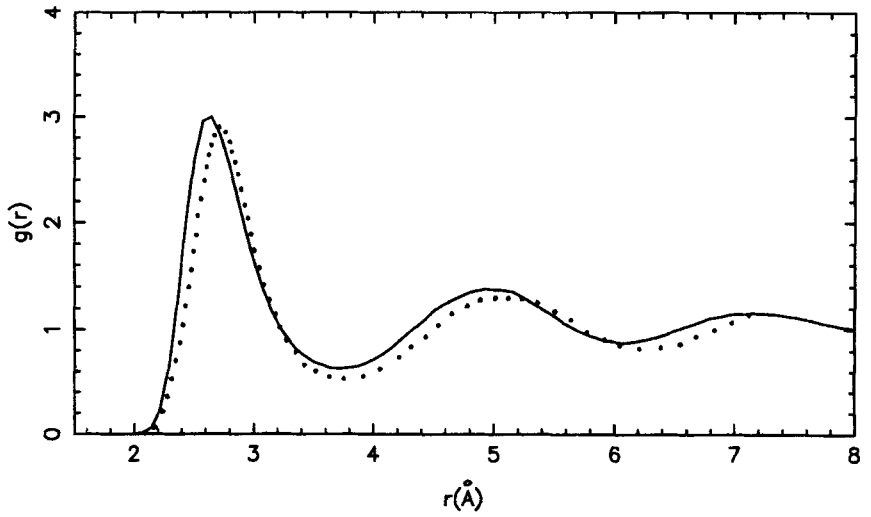

FIGURE 1 Pair correlation function $g(r)$ Al liquid metal. Full curves: MD simulation; dotted curves: experiment [21].

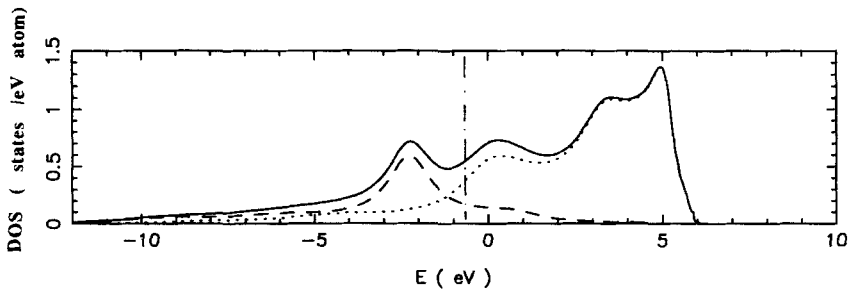

FIGURE 2 Calculated electronic density of states for the liquid Al metal. Full line corresponds to the total DOS, dashed line: s partial DOS and dotted line: p partial DOS.

elements in their closepacked metallic structure types (hcp or fcc) as described by Cressoni and Pettifor [16].

III.2. Structure of Liquid $Al_{80}Ni_{20}$ and $Al_{80}Mn_{20}$ Alloys

During the last few years, we have focused attention on the study of topological and chemical short-range order in $Al_{80}Mn_{20}$ and $Al_{80}Ni_{20}$ liquid alloys [17, 18] through the accurate determination of the partial pair correlation functions by neutron diffraction. The first distances in both Al-Al and M-M distributions (M = Mn or Ni) differ significantly in the two alloys, pointing out distinct topological ordering, the ordering extending to large distances in $Al_{80}Mn_{20}$ and being short range in $Al_{80}Ni_{20}$. This feature is emphasized in reciprocal space by the height difference observed for the first peak of the number-number structure factor $S_{NN}(q)$ in the Bhatia-Thornton formalism. Then it is important to know if our interactions are able to reproduce such differences. To simulate the liquid alloys, we consider a system of 691 Al atoms and 173 M atoms in a cubic box with periodic boundary conditions such that the densities of the two systems are equal to the experimental ones. The initial atomic positions are randomly chosen. The Bhatia-Thornton partial structure factors (PSF) shown in Figure 3 are based on averages of over the last 100 000 integration steps. They are perfectly in phase with the experimental curves and, more particularly, reproduce the experimental height of the first and second peaks of $S_{NN}(q)$ for both $Al_{80}Mn_{20}$ and $Al_{80}Ni_{20}$ liquids. The theoretical results presented here allows us to point out clues that indicate icosahedral order in the $S_{NN}(q)$ function of liquid $Al_{80}Mn_{20}$, which are absent for liquid $Al_{80}Ni_{20}$. These arguments are the following ones: (i) there is a large difference between both liquids in the height and the shape of the first peak

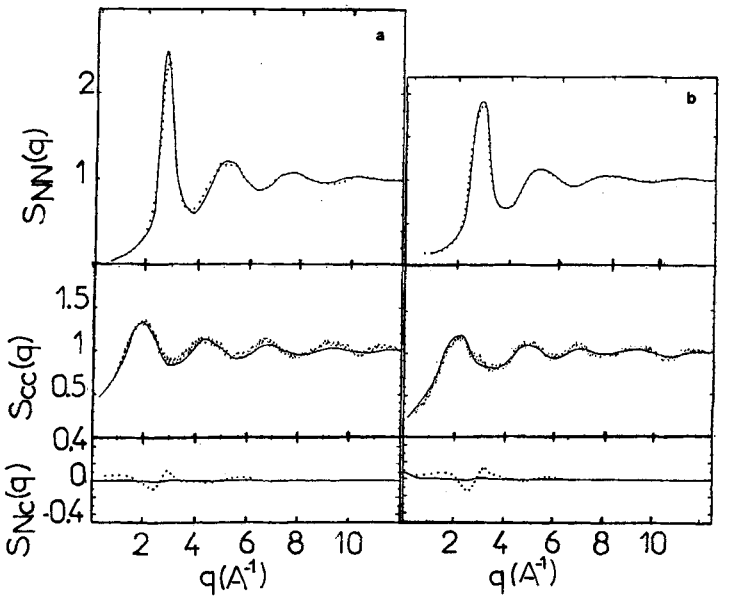

FIGURE 3 Comparison between theoretical and experimental Bhatia-Thornton partial structures for: (a) liquid $Al_{80}Mn_{20}$ (————) simulation, (·····) Ref. [17]; (b) liquid $Al_{80}Ni_{20}$ (————) simulation, (·····) Ref. [18].

($S_{NN}(q1) = 2.45$ with $q1 = 2.85$ Å^{-1} for $Al_{80}Mn_{20}$ and $S_{NN}(q1) = 1.92$ with $q1 = 2.95$ Å^{-1} for $Al_{80}Ni_{20}$). Since the ratio of atomic volumes of both species is similar in both systems (see functions $S_{Nc}(q)$), such a change in $S_{NN}(q)$ is attributed to a variation of the spacial extent ξ of topological ordering, ξ can be estimated from the breadth of the first peak of $S_{NN}(q)$ using the Scherrer particle broadening equation $2\pi/\Delta q_{NN}$. The values of ξ found for $Al_{80}Ni_{20}$ and $Al_{80}Mn_{20}$ are 7 and 10 Å, respectively; this means that atoms in $Al_{80}Mn_{20}$ are arranged roughly over one more interatomic distance than in $Al_{80}Ni_{20}$. (ii) The change in the second peak of $S_{NN}(q)$ is also quite visible; in particular, the second peak for $Al_{80}Ni_{20}$ is rounded while the one for $Al_{80}Mn_{20}$ has a flat top which from Ref.[19] could be suggestive of short-range icosahedral order. (iii) The height ratio between the second and the first peak S(q2)/S(q1) is quite different for both alloys; it is equal to 0.49 for $Al_{80}Mn_{20}$ while it is equal to 0.6 for $Al_{80}Ni_{20}$; for comparison the value of this ratio using a Landau description of short-range icosahedral order is 0.49 [20], very close to the ratio found in $Al_{80}Mn_{20}$ liquid. The first and second oscillations of the two functions $S_{cc}(q)$ are comparable in amplitude but those for $Al_{80}Ni_{20}$ are shifted towards

higher q. The spatial extent of chemical ordering deduced from the breadth of the first peak is about twice as small as the one of topological ordering.

All these results are confirmed by an analysis of the atomic arrangements between Aluminium and transition metal atoms in the first shell. The experimental distribution of the first distances Ni-Ni is split into two components at 2.36 Å and 2.98 Å. It is quite different from the distribution of the first distances Mn-Mn centered at 2.89 Å. Our results fail to reproduce the double-peak structure of contacts Ni-Ni in $Al_{80}Ni_{20}$ but give the general trend that the average first and second M-M distances are shorter in $Al_{80}Ni_{20}$. Indeed, we find r_{MM} equal to 2.55 Å in $Al_{80}Ni_{20}$ while it is equal to 2.86 Å in $Al_{80}Mn_{20}$. This difference cannot be attributed to the very small atomic size difference between Ni and Mn atoms (note that the nearest distances are 2.53 Å and 2.67 Å in Ni and Mn pure liquids [21]), and suggests different local structural arrangements. This is also supported by the first Al-Al distances significantly shorter than Mn-Mn contacts in $Al_{80}Mn_{20}$ and greater than Ni-Ni contacts in $Al_{80}Ni_{20}$. Experimental data give $r_{AlAl} = 2.82$ and 2.74 Å for $Al_{80}Ni_{20}$ and $Al_{80}Ni_{20}$ respectively, while theoretical analysis gives 2.78 and 2.76 Å. The distributions of the first heteroatomic pairs are centered at the same position (2.54 Å for experiments and 2.55 Å for calculations), which corresponds to short distances in comparison with M-M and Al-Al contacts. The fact that the topological short-range order is different in both alloys is also confirmed by the bond-angle distribution functions (see Fig. 4). For $Al_{80}Mn_{20}$, the calculated distribution shows a prominent peak near 63° and a broad maximum near 115°, very close to the icosahedral bond angles of $\theta = 63.5°$ and $\theta = 116.5°$. For $Al_{80}Ni_{20}$, the distribution is shifted towards smaller bond-angle values and the peak near 69° is less prominent than in $Al_{80}Mn_{20}$.

IV. ELECTRONIC DENSITY OF STATES OF LIQUID $Al_{80}Ni_{20}$ AND $Al_{80}Mn_{20}$ ALLOYS

These changes may now be traced back to the variation of the interatomic forces and of the electronic structure. As shown in Figure 5, the strong pd hybridization leads to a strong interaction between Al and M atoms for both liquids; the consequence is the formation of pairs of unlike atoms and short-bond distances in the Al-M pairs. But an important difference is between Ni-Ni and Mn-Mn interactions. The Mn-Mn interaction is found to be very small in comparison with Ni-Ni interactions and also Al-Al or Al-M interactions. It can be thought that it is the peculiar behaviour of

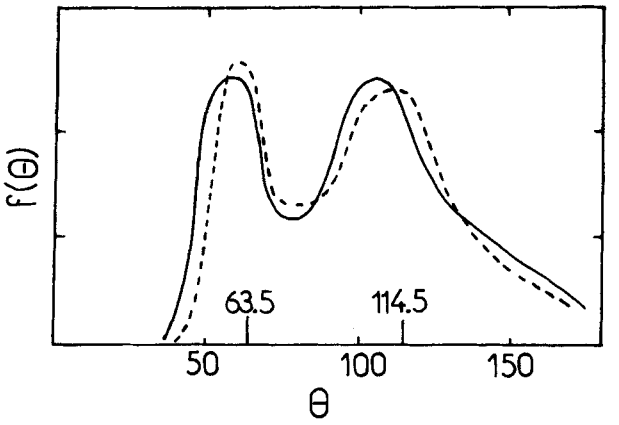

FIGURE 4 Calculated bond-angle distributions: (————) liquid $Al_{80}Mn_{20}$ (----------) liquid $Al_{80}Ni_{20}$.

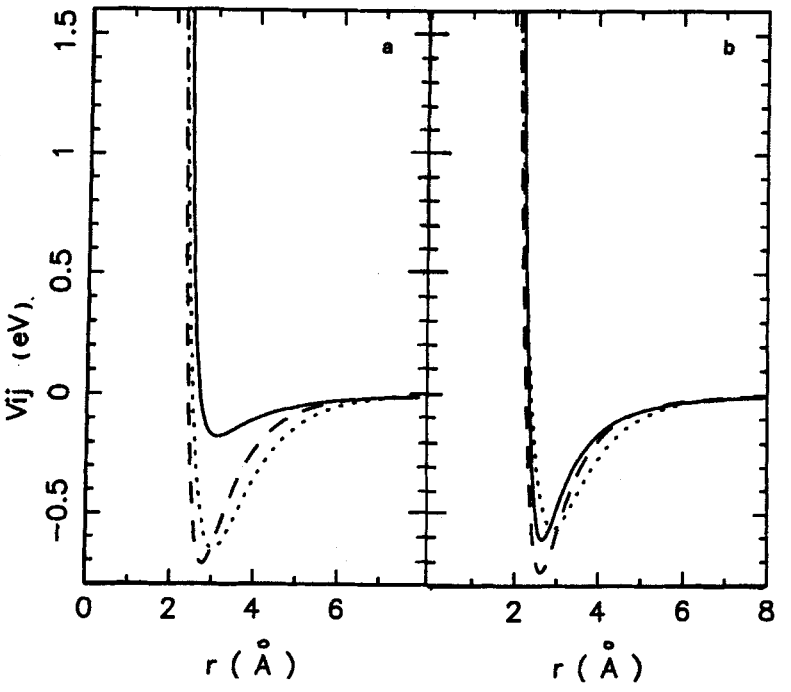

FIGURE 5 Tight-binding-bond potentials (eV); (————) M-M interaction, (----------) M-Al interaction, (·····) Al-Al interaction. (a) $Al_{80}Mn_{20}$; (b) $Al_{80}Ni_{20}$.

Mn-Mn interactions which can explain the difference of topological ordering in $Al_{80}Mn_{20}$ and $Al_{80}Ni_{20}$. The electronic density of states of both alloys are displayed in Figure 6. As for pure liquid metals, they are obtained usig the recursion method and 12 levels of the continued fraction. The shape of both DOSs is very similar and differs only by the position of the Fermi level; it is characterized by a narrow d band coupled with a broad sp band, the Fermi level being at the top of the d band of $Al_{80}Ni_{20}$ alloy. However, for $Al_{80}Mn_{20}$ alloy, the Fermi level is not located in the middle of the d band as for pure Mn [6] or for $Al_{60}Mn_{40}$ alloy [22]. Again, it is due to the peculiar behavior of Mn-Mn interactions in $Al_{80}Mn_{20}$ alloy. The overall shape of liquid $Al_{80}Mn_{20}$ alloy is very similar to that of α-(Al-Mn) compound as calculated by Fujiwara [23]. The major feature of the calculated DOS of α-(Al-Mn) compound is a dip or quasi-gap in the vicinity of the Fermi level; the quasi-gap was attributed to an antiresonance, with the resonance being the Fermi level. In the hypothetical binary Al-Mn case, the Fermi level resides at the lower-energy end of the quasi-gap. However, the origin of the DOS structure in the liquid $Al_{80}Mn_{20}$ alloy is quite different since the interatomic distances and coordination numbers in the first and second shells are different for the liquid and α phases [17]. The

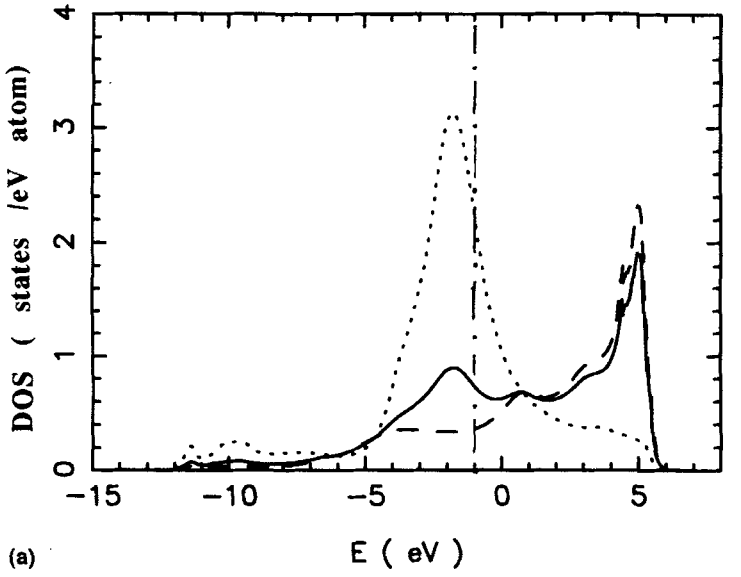

FIGURE 6 Calculated DOS for liquid alloys. (a) $Al_{80}Mn_{20}$; (b) $Al_{80}Ni_{20}$. Full line corresponds to the total DOS, dashed line: Mn or Ni partial DOS, and dotted line: Al partial DOS.

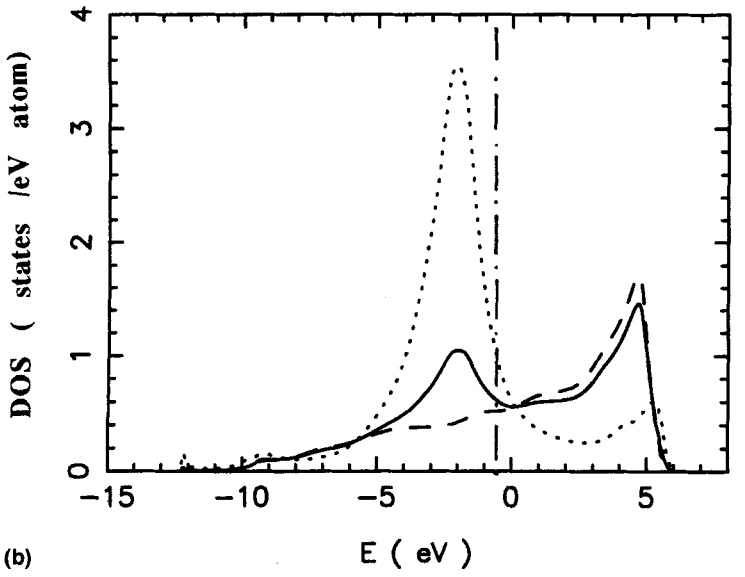

FIGURE 6 Continued.

most important feature is that Mn-Mn distance is longer in the liquid phase while, by contrast, the first Al-Al distance is shorter and the corresponding first-neighbour number is slightly larger. We think that in the liquid case, a strong Al p-Mn d hybridization but also an important Al p- Al p coupling due to the short Al-Al bond length are at the origin of the $Al_{80}Mn_{20}$-DOS structures.

IV. CONCLUSION

We have developed a new interatomic force field for disordered transition metal-Aluminium alloys which we believe contains an important improvement: the dependence of the pair interaction on the bond order determined by the strength of the pd hybridization. We have shown the applications to simulations of $Al_{80}Mn_{20}$ and $Al_{80}Ni_{20}$ liquid alloys are very promising. More particularly, it has been shown that topological and chemical short-range orders differ significantly in the two alloys. Our results allow us to point out clues that indicate icosahedral order in liquid $Al_{80}Mn_{20}$ which are absent for liquid $Al_{80}Ni_{20}$.

References

[1] Many-Atom Interaction in Solids, edited by Nieminen, R. M., Puska, M. J. and Manninen, M. J. (Springer, Berlin, 1990).

[2] Daw, M. S. and Baskes, I. (1984). Embedded-atom method: Derivation and application to impureties, surfaces, and other defects in metals, *Phys. Rev. B* **29**, 6443.

[3] Jacobsen, K. W., Norskov, J. K. and Puska, M. J. (1987). Interatomic interactions in the effective-medium theory, *Phys. Rev. B* **35**, 7423.

[4] Finnis, M. W. and Sinclair, J. E. (1984). A simple empirical N-body potential for transition metals, *Phil, Mag. A* **50**, 45.

[5] Pettifor, D. G. (1989). New Many-Body Potential for the Bond-Order, *Phys. Rev. Lett.* **63**, 2480; in Many-Atom Interactions in Solids, edited by Nieminen, R. M., Puska, M. J. and Manninen, M. J. Springer Verlag 1990, p. 64.

[6] Do Phuong, L., Nguyen Manh, D. and Pasturel, A. (1993). Effect of s-d hybridization on interatomic pair potentials of the 3d liquid transition metals, *J. Phys. Cond. Matter*, **5**, 1901; (1993). Microscopic Approach to the Structure of Liquid Alloys, *Phys. Rev. Lett*, **71**, 372.

[7] Sutton, A. P., Finnis, M. W., Pettifor, D. G. and Ohta, Y. (1988). The tight-binding bond model, *J. Phys. C* **21**, 35.

[8] Harris, J. (1985). Simplified Method for calculating the energy of weakly interacting fragments, *Phys. Rev. B* **31**, 1770.

[9] Foulkes, W. M. C. (1987). *Ph.D. Thesis*, University of Cambridge; Foulkes, M. W. C. and Haydock, R. (1989). Tight-binding models and density-functional theory, *Phys. Rev. B* **39**, 12520.

[10] Pettifor, D. G. and Aoki, M. (1991). Bonding and structure of Intermetallics: a new bond order potential, *Phil. Trans. R. Soc. Lond. A* **334**, 439.

[11] Mayou, D., Nguyen Manh, D., Pasturel, A. and Cyrot Lackmann, F. (1986). Model for the hybridization effect in disordered systems, *Phys. Rev. B* **33**, 3384.

[12] Nguyen Manh, D., Mayou, D., Morgan, G. J. and Pasturel, A. (1987). The Hall coefficient and the derivative of the density of states in amorphous metals, *J. Phys. F* **17**, 999.

[13] Harrison, W. A. Electronic Structure and the Properties of Solids, published by Freeman (San Fracisco, 1980).

[14] Goodwin, L., Skinner, A. J. and Pettifor, D. G. (1989). Generating Transferable Tight-Binding Parameters: Application to Silicon, *Europhys. Lett*, **9**, 701.

[15] Heermann, D. W. and Burkitt, A. N. (1991). Parallel Algorithms in Computational Science, Springer-Verlag, Berlin Heidelberg.

[16] Creesoni, J. C. and Pettiform, D. G. (1991). Theory of structural trends within the sp bonded elements, *J. Phys.: Condens. Matter*, **3**, 495.

[17] Maret, M., Pasturel, A., Senillou, C., Dubois, J. M. and Chieux, P. (1989). Partial structure factors of liquid $Al_{80}Mn_x(FeCr)_{1-x})_{20}$ alloys, *J. Phys. (Paris)* **50**, 295.

[18] Maret, M., Pomme, T., Pasturel, A. and Chieux, P. (1990). Structure of liquid $Al_{80}Ni_{20}$ alloy, *Phys. Rev.* B **42**, 1598.

[19] Sachdev, S. and Nelson, D. R. (1985). Order in metallic glasses and icosahedreal cyrstals, *Phys. Rev.* B **32**, 4592.

[20] Sachdev, S. and Nelson, D. R. (1984). Theory of the Structure Factor of Metallic Glasses, *Phys. Rev. Lett.* **53**, 1947.

[21] Waseda, Y. (1976). Liquid Metals, *IOP Conf. Proc. Ser.* No. **30**, edited by Evans, R. and Greenwood, D. A. (IOP, Bristol, 1977), p. 230; (1981). The Structure of Non-crystalline Materials-Liquids and Amorphous Solids, New York, Mc Graw-Hill.

[22] Do Phuong, L., Nguyen Manh, D. and Pasturel, A. (1994). Molecular dynamics of topological and chemical orders in liquid $Al_{1-x}Mn_x$ alloys, *J. Phys. Cond. Matter*, **6**, 2853.

[23] Fujiwara, T. (1989). Electronic structure in the Al-Mn alloy crystalline analog of quasicrystals, *Phys. Rev.* B **40**, 942.